Near-field probing of slow Bloch modes on photonic crystals with a nanoantenna

T-P. Vo,[1] M. Mivelle,[3,5] S.Callard,[1,*] A. Rahmani,[2] F. Baida,[3] D. Charraut,[3] A. Belarouci,[1] D. Nedeljkovic,[4] C.Seassal,[1] G.W. Burr,[5] and T. Grosjean[3,6]

[1] *Université de Lyon, Institut des nanotechnologies de Lyon INL-UMR 5270,CNRS, Ecole Centrale de Lyon, Avenue Guy de Collongue, F-69134 Cedex, France*
[2] *School of Mathematical Sciences, University of Technology, Sydney, NSW 2007, Australia*
[3] *Département d'Optique P.M. Duffieux,Institut FEMTO-ST, UMR CNRS 6174, Université de Franche-Comté,16 route de Gray, 25030 Besanon cedex, France*
[4] *Lovalite s.a.s.18 rue Alain Savary, 25000 Besanon, France*
[5] *IBM Almaden Research Center, D2/K13E,650 Harry Road, San Jose, California 95120, USA*
[6] *thierry.grosjean@univ-fcomte.fr*
[*] *segolene.callard@ec-lyon.fr*

Abstract: We study the near-field probing of the slow Bloch laser mode of a photonic crystal by a bowtie nano-aperture (BNA) positioned at the end of a metal-coated fiber probe. We show that the BNA acts as a polarizing nanoprobe allowing us to extract information about the polarization of the near-field of the slow-light mode, without causing any significant perturbation of the lasing process. Near-field experiments reveal a spatial resolution better than $\lambda/20$ and a polarization ratio as strong as 110. We also demonstrate that the collection efficiency is two orders of magnitude larger for the BNA than for a 200 nm large circular aperture opened at the apex of the same metal-coated fiber tip. The BNA allows for overcoming one of the main limitations of SNOM linked to the well-known trade off between resolution and signal-to-noise ratio.

OCIS codes: (180.4243) Near-field microscopy; (130.5440)Polarization-selective devices; (350.4238) Nanophotonics and photonic crystal.

References and links

1. J. Joannopoulos, S. Johnson, J. Winn, and R. Meade, *Photonic Crystals: Molding the Flow of Light* 2nd ed. (Princeton University Press, 2008).
2. S. Bozhevolnyi, V. Volkov, T. Søndergaard, A. Boltasseva, P. Borel, and M. Kristensen, "Near-field imaging of light propagation in photonic crystal waveguides: Explicit role of bloch harmonics," Phys. Rev. B **66**, 235204 (2002).
3. R. Wuest, D. Erni, P. Strasser, F. Robin, H. Jackel, B. C. Buchler, A. F. Koenderink, V. Sandoghdar, and R. Harbers, "A "standing-wave meter" to measure dispersion and loss of photonic-crystal waveguides," Appl. Phys. Lett. **87**, 261110 (2005).
4. P. Kramper, M. Kafesaki, C. Soukoulis, A. Birner, F. Müller, U. Gösele, R. Wehrspohn, J. Mlynek, and V. Sandoghdar, "Near-field visualization of light confinement in a photonic crystal microresonator," Opt. Lett. **29**, 174–176 (2004).
5. N. Louvion, D. Gérard, J. Mouette, F. de Fornel, C. Seassal, X. Letartre, A. Rahmani, and S. Callard, "Local observation and spectroscopy of optical modes in an active photonic-crystal microcavity," Phys. Rev. Lett. **94**, 113907 (2005).
6. M.-P. Bernal, M. Roussey, and F. Baida, "Near- and far-field verification of electro-optic effect enhancement on a tunable lithium niobate photonic crystal," J. Microscopy **229**, 264–269 (2008).

#158651 - $15.00 USD Received 23 Nov 2011; revised 26 Jan 2012; accepted 31 Jan 2012; published 3 Feb 2012

7. N. Fabre, L. Lalouat, B. Cluzel, X. Melique, D. Lippens, F. de Fornel, and O. Vanbesien, "Optical near-field microscopy of light focusing through a photonic crystal flat lens," Phys. Rev. Lett. **101**, 073901 (2008).
8. T.-P. Vo, A. Rahmani, A. Belarouci, C. Seassal, D. Nedeljkovic, and S. Callard, "Near-field and far-field analysis of an azimuthally polarized slow bloch mode microlaser," Opt. Express **18**, 26879–26886 (2010).
9. C. Girard and E. Dujardin, "Near-field Optical properties of top-down and bottom-up nanostructures", J. Opt. A. **8**, S73–S86, (2006).
10. H. H. Tao ,R. J. Liu,Z. Y. Li ,S. Feng,Y. Z. Liu , C. Ren,B. Y. Cheng, D. Z. Zhang ,H. Q. Ma ,L. A. Wu and Z. B. Zhang, "Mapping of complex optical field patterns in multimode photonic crystal waveguides by near-field scanning optical microscopy", Phys. Rev. B **74**, 205111 (2006).
11. M. Burresi, R. J. P. Engelen, A. Opheij, D. van Oosten, D. Mori, T. Baba, and L. Kuipers, "Observation of polarization singularities at the nanoscale," Phys. Rev. Lett. **102**, 033902 (2009).
12. S. Vignolini, F. Intonti, F. Riboli, D. S. Wiersma, L. Balet, L. H. Li, M. Francardi, A. Gerardino, A. Fiore, and M. Gurioli, "Polarization-sensitive near-field investigation of photonic crystal microcavities," Appl. Phys. Lett. **94**, 163102 (2009).
13. L. Novotny and B. Hecht, *Principle of Nano-Optics* (Cambridge University Press, 2006).
14. H. A. Bethe, "Theory of diffraction by small holes," Phys. Rev. **66**, 163–182 (1944).
15. C. J. Bouwkamp, "Diffraction theory," Rep. Prog. Phys. **17**, 35 (1954).
16. Y.R.Samii and R. Mittra, IEEE Trans. Antennas and Propagation **25**, 180–187 (1977).
17. E. Bortchagovsky, G. Colas des Francs, D. Molenda, A. Naber, and U. Fischer, "Transmission of an obliquely incident beam of light through small apertures in a metal film," Appl. Phys. B. **84**, 49–53 (2006).
18. U. Schroter and A. Dereux, "Surface plasmon polaritons on metal cylinders with dielectric core," Phys. Rev. B **64**, 125420 (2001).
19. E. Devaux, A. Dereux, E. Bourillot, J. Weeber, Y. Lacroute, J. Goudonnet, and C. Girard, "Local detection of the optical magnetic field in the near zone of dielectric samples," Phys. Rev. B **62**, 10504–10514 (2000).
20. J. Greffet and R. Carminati, "Image formation in near-field optics," Prog. Surf. Sci. **56**, 133–237 (1997).
21. D. Vanlabeke and D. Barchiesi, "Probes for scanning tunneling optical microscopy - a theoretical comparison," J. Opt. Soc. Am. **10**, 2193–2201 (1993).
22. M. Notomi, "Manipulating light with strongly modulated photonic crystals," Rep. Prog. Phys. **73**, 096501 (2010).
23. P. Viktorovitch, B. Ben Bakir, S. Boutami, J.-L. Leclercq, X. Letartre, P. Rojo-Romeo, C. Seassal, M. Zussy, L. Di Cioccio, and J.-M. Fedeli, "3D harnessing of light with 2.5D photonic crystals," Laser Photon. Rev. **4**, 401–413 (2010).
24. F. Raineri, C. Cojocaru, R. Raj, P. Monnier, A. Levenson, C. Seassal, X. Letartre, and P. Viktorovitch, "Tuning a two-dimensional photonic crystal resonance via optical carrier injection," Opt. Lett. **30**, 64–66 (2005).
25. P. Bharadwaj, B. Deutsch, and L. Novotny, "Optical antennas," Adv. Opt. Photon. **1**, 438–483 (2009).
26. R. Grober, R. Schoelkopf, and D. Prober, "Optical antenna: Towards a unity efficiency near-field optical probe," Appl. Phys. Lett. **70**, 1354–1356 (1997).
27. P. Schuck, D. Fromm, A. Sundaramurthy, G. Kino, and W. Moerner, "Improving the mismatch between light and nanoscale objects with gold bowtie nanoantennas," Phys. Rev. Lett. **94**, 017402 (2005).
28. L. Wang, E. X. Jin, S. M. Uppuluri, and X. Xu, "Contact optical nanolithography using nanoscale C-shaped apertures," Opt. Express **14**, 9902–9908 (2006).
29. I. A. Ibrahim, M. Mivelle, T. Grosjean, J. T. Allegre, G. W. Burr, and F. I. Baida, "Bowtie-shaped nanoaperture: a modal study," Opt. Lett. **35**, 2448–2450 (2010).
30. M. Mivelle, I. A. Ibrahim, F. Baida, G. W. Burr, D. Nedeljkovic, D. Charraut, J.-Y. Rauch, R. Salut, and T. Grosjean, "Bowtie nano-aperture as interfacebetween near-fields and a single-modefiber," Opt. Express **18**, 15964–15974 (2010).
31. S.-H. Kwon and Y.-H. Lee, "High index-contrast 2d photonic band edge laser," IEICE. Trans. Electron. **E.87**, 308–315 (2004).
32. K. Sakai, E. Miyai, T. Sakaguchi, D. Ohnishi, T. Okano, and S. Noda, "Lasing band-edge identification for a surface-emitting photonic crystal laser," IEEE J. Sel. Areas Commun. **23**, 1335–1340 (2005).
33. E. Miyai, K. Sakai, T. Okano, W. Kunishi, D. Ohnishi, and S. Noda, "Lasers producing tailored beams," Nature **441**, 946 (2006).
34. L. Wang and X. Xu, "High transmission nanoscale bowtie-shaped aperture probe for near-field optical imaging," Appl. Phys. Lett. **90**, 261105 (2007).
35. R. Bachelot, C. Ecoffet, D. Deloeil, P. Royer, and D. Lougnot, "Integration of micrometer-sized polymer elements at the end of optical fibers by free-radical photopolymerization," Appl. Opt. **40**, 5860–5871 (2001).
36. A.Taflove and S. Hagness, *Computational Electrodynamics: The Finite-Difference Time-Domain Method*, 3rd ed. (Artech House: Boston, 2005).
37. L. Novotny, M. Beversluis, K. Youngworth, and T. Brown, "Longitudinal field modes probed by single molecules," Phys. Rev. Lett. **86**, 5251–5254 (2001).
38. T. Grosjean, I. A. Ibrahim, M. A. Suarez, G. W. Burr, M. Mivelle, and D. Charraut, "Full vectorial imaging of electromagnetic light at subwavelength scale," Opt. Express **18**, 5809–5824 (2010).
39. C. Monat, C. Seassal, X. Letartre, R. Regreny, P. Rojo-Romeo, P. Viktorovitch, M. d'Yerville, D. Cassagne,

#158651 - $15.00 USD Received 23 Nov 2011; revised 26 Jan 2012; accepted 31 Jan 2012; published 3 Feb 2012

J. Albert, E. Jalaguier, S. Pocas, and B. Aspar, "InP-based two-dimensional photonic crystal on silicon: In-plane Bloch mode laser," Appl. Phys. Lett. **81**, 5102–5104 (2002).
40. G. Le Gac, A. Rahmani, C. Seassal, E. Picard, E. Hadji, and S. Callard, "Tuning of an active photonic crystal cavity by an hybrid silica/silicon near-field probe," Opt. Express **17**, 21672–21679 (2009).
41. S. I. Bozhevolnyi and E. A. Bozhevolnaya, "Near-field imaging of the interference pattern of counterpropagating evanescent waves," Opt. Lett. **24**, 747–749 (1999).
42. S. I. Bozhevolnyi and B. Vohnsen, "Near-field imaging of optical phase and its singularities", Opt. Commun. **212** 217–23 (2002).
43. L. Neumann,Y. Pang, A. Houyou, M. L. Juan, R. Gordon, and N.F. van Hulst, "Extraordinary optical transmission brightens near-field fiber probe," Nano Lett. **11**, 365–360 (2011).
44. A. Belarouci, T. Benyattou, X. Letartre, and P. Viktorovitch, "3D light harnessing based on coupling engineering between 1D-2D Photonic Crystal membranes and metallic nano-antenna," Opt. Express **18**, A381–A394 (2010).
45. M. Barth, S. Schietinger, S. Fischer, J. Becker, N. Nüsse, T. Aichele, B. Löchel, C. Sönnichsen, and O. Benson, "Nanoassembled plasmonic-photonic hybrid cavity for tailored light-matter coupling," Nano Lett. **10**, 891–895 (2010)

1. Introduction

For more than fifteen years, 2D photonic crystals (PCs) have been used to control optical fields down to the nanoscale [1]. Given the complex, vectorial nature of optical fields associated with subwavelength structures, a complete and precise knowledge of the electromagnetic field near a PC is difficult to gain. While theoretical models can predict vector field maps near an ideal PC structure, finding a reliable experimental technique to study the vectorial nature of confined optical fields near an actual 2D PC device remains both highly desirable and challenging, especially considering how difficult it is for a near-field probe not to perturb the optical signature of the sample . Beyond the novel experimental insight given by mapping the polarization state of the fields, a more precise analysis of the optical properties of a PC would make it possible to better assess the performance of a device, by comparing not only spatial intensity profiles but also local polarization states with theoretical models. With this in prospect, scanning Near-field Optical Microscopy (SNOM) has been widely used to investigate the optical properties of 2D PC structures [2–10] including to access vectorial information about the optical modes [11, 12]. However, SNOM probes used in these experiments are not ideal for the accurate and reliable measurement of optical near-fields. On the one hand, the signal detected by conventional metal-coated aperture and apertureless probes is usually a "mixture" of electric and magnetic components. In this case, the probe apex can be viewed as nanoscale optical antenna [13] with electric and magnetic dipole moments which convert both electric and magnetic near-field information into free space propagating modes, albeit with a rather low conversion efficiency [14–19]. This is a serious issue for the accurate interpretation of results since the subwavelength spatial profiles of the electric and magnetic fields may be different. Only bare dielectric tips, which can be represented by an electric dipole moment only, are known to selectively collect the electric optical field [20, 21], but at the cost of a modest spatial resolution. On the other hand, conventional SNOM probes have difficulties faithfully mapping the near-field of 2D PCs showing a strong vertical emission, i.e. operating at or near the Γ-point (center) of the Brillouin zone [22–24]. It has been shown that the nature of the coupling between the probe and the slow Bloch mode (SBM) is very critical, in particular due to the large propagating component of the field which interferes with the evanescent contribution and swamps some of the finer details [8].

Recently, resonant nanoantennas have been proposed as a way of establishing a two-way communication channel between optical nano-structures and free space radiation modes, thus enhancing dramatically light-matter interaction down to the nanoscale [25]. Among the various configurations of nanoantennas proposed so far, the bowtie [26, 27] and bowtie-aperture nanoantennas [28, 29] were shown to be very efficient designs for creating highly confined and enhanced electric optical fields in the small gap between their two triangular metal particles.

#158651 - $15.00 USD Received 23 Nov 2011; revised 26 Jan 2012; accepted 31 Jan 2012; published 3 Feb 2012

Their resonant optical properties, defined by a huge optical capacitive effect within the air gap, are governed by an electric dipole moment oriented along the metal triangles. This means that these nanoantennas interact mainly with a single vector component of the electric field and light re-emission by the antenna is due to electric optical processes. As detailed in a recent theoretical work, BNAs may be used as high resolution polarizing nanocollectors with little sensitivity to the magnetic optical fields [30].

In this article, we propose to use BNAs integrated at the apex of SNOM fiber tips as nanoprobes for mapping the vectorial components of the electric near-field of 2D-PC slow Bloch laser mode. We consider surface addressable PC exploiting SBMs emitting in the vertical direction, i.e. operating at the Γ-point of the Brillouin zone. Near this point, low curvature flat bands give rise to delocalized, stationary optical modes. These modes have attracted much attention recently as they lead to versatile photonic structures not restricted to operate in the traditional in-plane, wave-guiding regime but suitable for coupling to free-space radiation [31, 32]. SBMs at the Γ-point have already been exploited to directly achieve vertical laser emission with peculiar polarization states, such as azimuthal or radial polarizations [8, 33]. So far, the investigation of the potential of BNAs as near-field optical nanoprobes has been limited to the nano-imaging of simple test-objects and only their resolution and collection efficiency have been investigated [30, 34]. The issue of the local and vectorial imaging of the modes of complex nanophotonic structures, such as photonic crystal based devices, with a nanoantenna tip has not been addressed yet. Here, we experimentally demonstrate the potential of BNAs integrated at the apex of SNOM fiber probes for polarization-resolved optical mapping of the electric field with unprecedented signal-to-noise ratios and without perturbation of the laser emission. We also show that the resonance properties of the BNA lead to high resolution abilities in SNOM imaging with high collection efficiencies, in opposition to conventional circular nano-apertures for which any improvement of resolution is associated with a loss of collection efficiency.

2. Design and fabrication

2.1. Nanoantenna probe

In order to produce the BNA-on-tip, polymer tips (30μm) are first grown by photopolymerization at the cleaved end facet of a monomode (1.55 micron wavelength) glass fiber [35]. Next, the probes are metal coated with a few nanometer thick titanium adhesion layer followed by a 100 nm thick aluminum layer. Aluminum is chosen for its high conductivity at infrared frequencies leading to a strong antenna effect. Finally, a 220 nm wide BNA with square gap smaller than 40 nm and 45° flare angles is opened at the rounded apex of the tip by Focused Ion Beam (FIB) milling. Figure 1(a) and Fig. 1(b) display scanning electron micrographs of a resulting fiber device. The BNA is designed to be resonant at λ=1.55 microns when it is in contact with an air/InP interface. The design process is performed using three dimensional Finite Difference in Time Domain method (3D FDTD) [36]. Figure 1(c) shows the collection spectrum of the BNA probe placed 10 nm away from a semi-infinite medium of InP, in air. Note that the presence of this high-index semi-infite medium has a strong impact on the resonance properties of the BNA and has to be taken into account in the design of the BNA. In the simulation, the BNA is excited by a single dipole positioned 5 nm below the gap of the BNA, orthogonal to the common median of the triangles, and radiating a single temporal pulse. The time-varying Poynting vector flow is calculated inside the probe, integrated over a transverse cross-section located 2 microns away from the BNA. The spectrum of the collected power is calculated by Fourier-transforming this result. The BNA resonance, of quality factor about 6, is large enough to allow an efficient nanocollection of the optical signal at wavelengths ranging from 1450 nm to 1650 nm. The polarization ratio of the BNA probe with dipolar excitation has been predicted

#158651 - $15.00 USD Received 23 Nov 2011; revised 26 Jan 2012; accepted 31 Jan 2012; published 3 Feb 2012

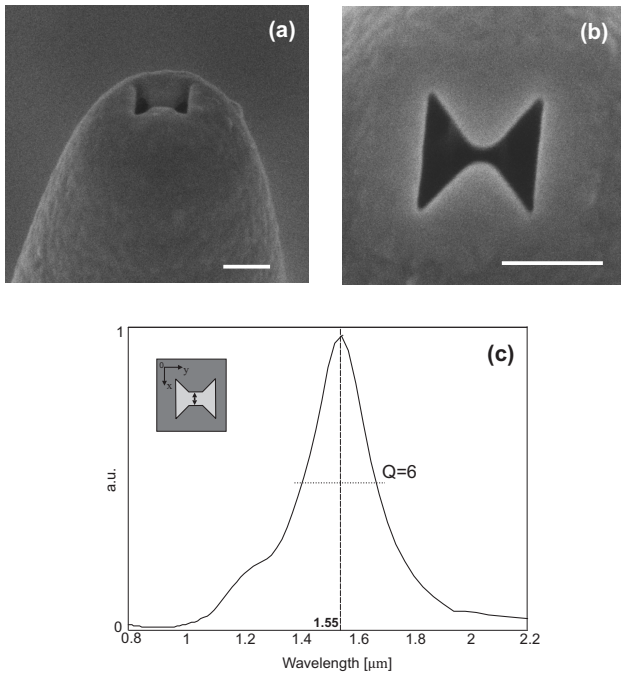

Fig. 1. (a,b) SEM images of the probe-integrated BNA : (a) side view of the tip apex, (b) zoom of the probe apex on which the BNA is opened (scale bars : 200 nm), (c): simulation of the collection spectrum of the BNA-on-tip with a dipolar excitation within the gap. The nanoprobe is studied in contact to an air/InP interface (inset : dipole orientation with respect to the BNA).

to be about 1:170 in a previous study but can vary with the nature of the optical fields probed by the BNA [30].

2.2. Photonic crystal structure

The PC design consists of a honeycomb lattice of cylindrical air holes (with a lattice parameter A=730 nm and a 245 nm hole diameter) patterned in a 240 nm thick InP slab bonded on top of a transparent SiO_2 substrate (see Fig. 2(a) and Fig. 2(c)). The PC structure is designed to support a low curvature band-edge mode at the Γ-point of the first Brillouin zone. This SBM radiates in the vertical direction and will be labelled M-mode, in reference with the monopolar symmetry of the magnetic field [8]. The light distribution of the M-mode at the surface of the 2D-PC was modelled using 3D FDTD and is presented in Fig. 2(a). In the simulation, the mode expansion is limited by the edges of the PC-structure. The light intensity is maximum at the center of the PC and its global envelope is gaussian. In addition, simulations indicate that the intensity is distributed in each unit cell of the honeycomb lattice in a "doughnut" shape of about 260 nm of outer radius and 90 nm of inner radius (Fig. 2(b)). The polarization of the electric field inside each unit cell is azimuthal : the zero of the intensity of the field at the center of each hexagon is due to a phase singularity. These axially-polarized nano-doughnut beams are actually ideal test beds for assessing the polarization sensitivity of nano-objects such as single molecules [37] or near-field probes [38]. The photonic crystal are 40μm by 40μm wide and are patterned into the InP layer using e-beam lithography and reactive ion etching [39]. Four InAsP quantum wells, separated by InP barrier layers, are embedded at the center of the semiconductor film. The

#158651 - $15.00 USD Received 23 Nov 2011; revised 26 Jan 2012; accepted 31 Jan 2012; published 3 Feb 2012

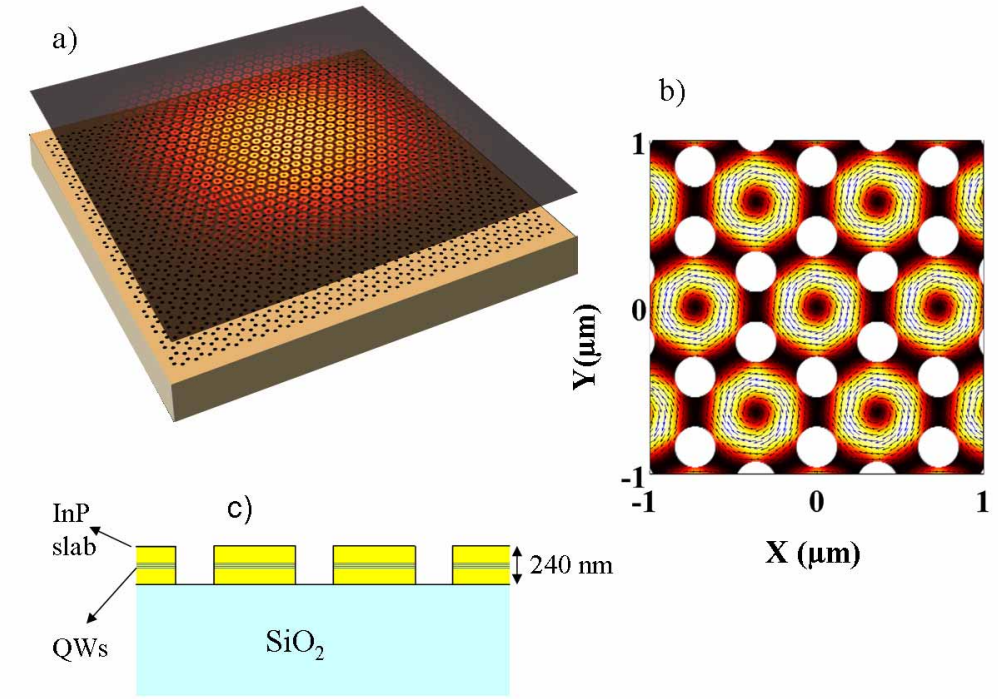

Fig. 2. (a)Overview of the PC structure with the 3D FDTD simulation of the monopolar mode at the surface of a 2D-PC slab honeycomb structure : the normalized field intensity ($|E_x|^2+|E_y|^2$) is computed at the surface of the PC at λ =1602 nm.(b) Detail (2μm x 2μm) of the computed map of (a). Arrows represent the field polarisation orientation. (c) Vertical cross section of the sample

photoluminescence from the quantum wells (QWs) occurs over a broad spectral range between 1250 nm and 1650 nm. The 2DPC structures are designed to exhibit modes in the wavelength range of the QWs emission. The BNA spectral properties have also been engineered to overlap this spectral range.

3. Experimental set up

PC structures are optically pumped at λ =780 nm with a laser diode. In our set-up, we used an inverted microscope to pump the sample from the back side. The pump laser beam is focused onto the 2D-PC through the silica substrate with a corrected objective of numerical aperture (NA) equal to 0.75. Its position and shape are perfectly controlled : the excitation spot at the PC surface has a Gaussian profile and a surface area smaller than 10 μm by 10 μm (Fig. 3(a)). Simultaneously to far-field measurements, SNOM acquisitions are carried out in collection mode with a stand alone commercial head (NT-MDT SMENA) positioned at the top of the inverted microscope (detailed experimental set up can be found in [8]). Near-field images are recorded by collecting locally the optical information through the BNA fiber probe during raster scan across the PC structure. After collection by the probe, the pump light is filtered out by a long-pass filter (cutoff wavelength 1100 nm). A monochromator with a 1 nm resolution in the infrared, and a thermo-electrically cooled InGaAs photodetector are used for spectral

#158651 - $15.00 USD Received 23 Nov 2011; revised 26 Jan 2012; accepted 31 Jan 2012; published 3 Feb 2012

measurements. The distance between the probe and the sample is regulated using a non-optical shear-force feedback loop that keeps the probe less than 10 nm away from the sample. In our experiments, the orientation of the BNA is kept fixed with respect to the scan direction. To probe the different polarization components of the SBM, we simply rotate the sample. For comparison, near-field measurements have also been conducted with conventional SNOM probes: metallized probes with 200 nm large circular aperture. These apertures have been engineered at the apex of the same polymer tips that we use for the BNA.

4. Results and discussion

Under these excitation conditions, the M-mode is lasing. The laser beam emitted by the PC structure is imaged in far-field with the same objective coupled to an infrared camera (Fig. 3(b)): it takes the shape of a large doughnut and is found to be azimuthally polarized [8]. Figure 3 shows the topographic shear-force images of the structure and the optical near-field images recorded with the BNA-on-tip at the lasing wavelength λ =1611 nm. In this study, the BNA is oriented along two characteristic orthogonal axes of the honeycomb lattice unit cell, called *x*-axis and *y*-axis in the following (see insets of Fig. 3). In Fig. 3(c) and Fig. 3(e), the two triangles of the BNA-on tip are aligned with the *y*-axis whereas in Fig. 3(d) and Fig. 3(f), the sample has been rotated by 90° so that the BNA-on-tip is oriented along the *x*-axis. The hole pattern of the 2D-PC is clearly visible in Fig. 3(c) and Fig. 3(d) which demonstrates the ability of the tip to yield the correct topography of the PC. Figure 3(e) and Fig. 3(f) show that the optical contrast is excellent for the two orientations of the BNA tip. Laser emission is achieved in both configurations, which demonstrates that any loss induced by the presence of the BNA-on-tip in the near-field of the PC is small enough not to hinder the lasing process. Moreover, the lasing wavelength and the far-field pattern of the laser mode remain unchanged irrespective of whether the BNA tip is present. This is a very good indication that the tip does not perturb the M-mode. Unlike cavity (defect) modes, large stationary modes such as slow band-edge mode are more robust to small perturbations such as a single BNA-on-tip [40].

Figure 4 shows the comparison between simulation (3D FDTD) and experiment (SNOM) for the electric field intensity of the M-mode mode across a few unit cells of the PC. The SNOM images over a given area are captured with either a BNA or a 200 nm large circular nano-aperture. Figure 4(a) and Fig. 4(b) show the simulation of the total electric intensity ($|E_x|^2 + |E_y|^2$) and the near-field optical image recorded with a 200 nm aperture tip, respectively. The circular aperture tip is able to resolve the light distribution inside a unit cell, revealing the doughnut shape of the optical field [8]. The convenional-tip resolution is estimated by comparing the computed and the experimental maps and found to be of the order of $\lambda/7$. This figure is in good agreement with the aperture size which is about 200 nm. Note that the sensitivity of the SNOM tips to the electric and/or magnetic optical fields cannot be determined experimentally with the SBM for which the transverse electric and transverse magnetic intensities overlap and lead to the same light patterns.

Figure 4(c) and Fig. 4(e) display the simulations of the intensity distributions $|E_x|^2$ and $|E_y|^2$, respectively. The corresponding SNOM images with the BNA tip oriented along the *x*-axis and *y*-axis are reported in Fig. 4(d) and Fig. 4(f), respectively. Experimental maps are recorded on the same structure as in Fig. 3. The theoretical results are in excellent agreement with the experimental results despite the fact that the tip is not taken into account in the simulations. It clearly demonstrates the ability of the nanoantenna to provide accurate subwavelength information on the vectorial properties of the SBM. Note that the orientation of the BNA-on-tip with respect to the PC can be directly inferred from the experimental acquisitions because of the azimuthal polarization [37,38].To estimate the performances of the BNA-on-tip as polarizing nanocollector, cross sections of Fig. 4(d) and Fig. 4(f), taken along the *x* and *y*-axis over a unit cell ($\approx 1.5\mu m$

#158651 - $15.00 USD Received 23 Nov 2011; revised 26 Jan 2012; accepted 31 Jan 2012; published 3 Feb 2012

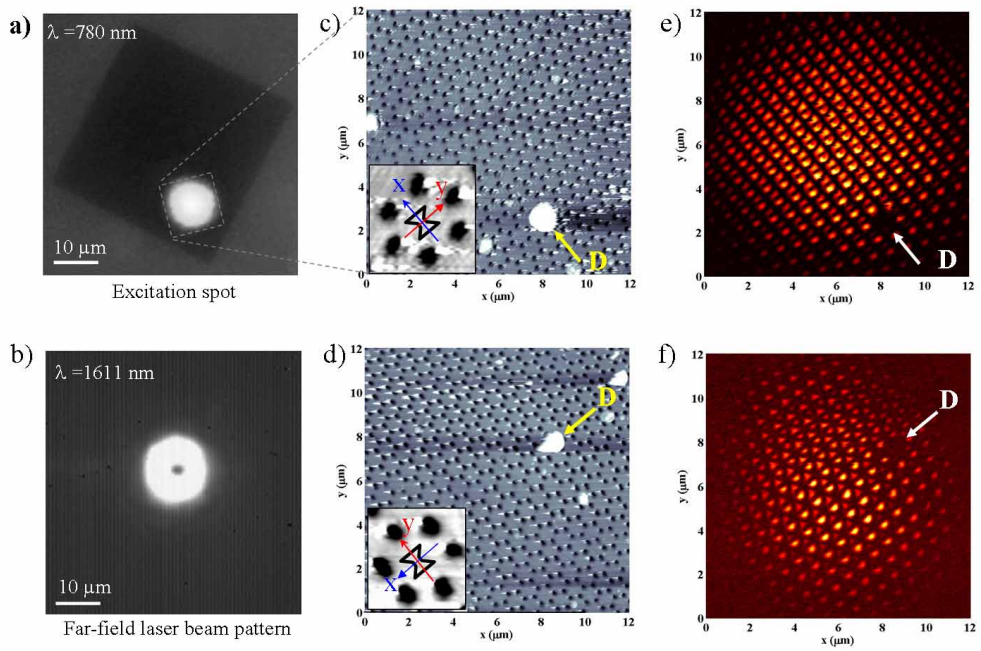

Fig. 3. (a) Position of the excitation spot (diameter≈10μm, λ =780nm) with respect to the 2D-PC structure (40x40μm^2) (image recorded in far-field with a CCD camera). (b) Far-field image of the lasing mode with a corrected objective (NA=0.75) focused at the surface of the 2D-PC. (c) and (e): topographic (shear-force) and SNOM images at the surface of the PC with the BNA tip oriented along the *y*-axis, respectively (see figure inset). (d) and (f) topographic (shear-force) and SNOM images at the surface of the PC with the BNA tip oriented along the *x*-axis, respectively (see figure inset). SNOM images are recorded at the lasing wavelength λ =1611 nm. The orientation of the sample in (d) and (f) is rotated by 90° with respect to (c) and (e). The presence of a large particle, identified as "D" in (c,d) and (e,f), indicates that the two series of near-field images have been recorded in the same area. BNA orientation kept unchanged in this study, as shown in figure insets. Number of pixels is 400x400 for near-field maps.

#158651 - $15.00 USD Received 23 Nov 2011; revised 26 Jan 2012; accepted 31 Jan 2012; published 3 Feb 2012

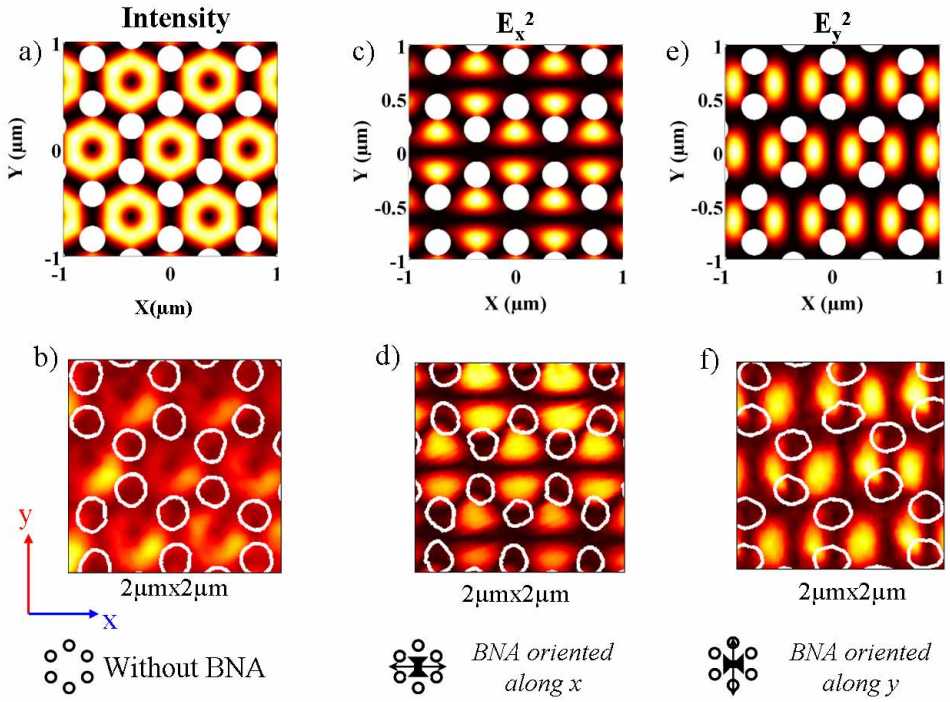

Fig. 4. 3D-FDTD simulations of the electric intensity of the SBM vs. experimental near-field images of the M-mode recorded by SNOM with BNA and conventional aperture tips. (a,c,e) simulation of the spatial profile of the electric field of the SBM (λ=1602nm): (a) total intensity $|E_x|^2+|E_y|^2$, (c) intensity $|E_x|^2$ of the component of the electric field parallel to the *x*-axis and (e) intensity $|E_y|^2$ of the component of the electric field parallel to the *y*-axis. White discs represent the holes of the PC. (b,d,f) SNOM images at the emission wavelength of the PC laser (λ =1611 nm): (b) with a conventional aperture tip, (d) and (f) images recorded with a BNA-on-tip oriented along the *x* and *y*-axis, respectively. White circles represent the real PC geometry inferred from the topographic image. Numbers of pixels are 115x115 for (d), 58x58 for (f) and (b).

#158651 - $15.00 USD Received 23 Nov 2011; revised 26 Jan 2012; accepted 31 Jan 2012; published 3 Feb 2012

), are plotted in Fig. 5(a) and Fig. 5(b), respectively. The profile of $|E_x|^2$ (Fig. 5(a)) along the *x*-axis exhibits two peaks, as predicted by theory, whereas its profile along the *y*-axis remains close to zero. The opposite behavior is shown for $|E_y|^2$ in Fig. 5(b): the intensity profile remains close to zero along the *x*-axis and oscillates along the *y*-axis. These results demonstrate that the measurement of $|E_x|^2$ is not "contaminated" by E_y, and vice versa. Actually, the polarization ratio is difficult to evaluate as the remnant cross-polarized signal is of the order of the background ($0.110mV \pm 0.015mV$ for Fig. 5(a)). The background fluctuations therefore limit the measurements of the real polarization ratio. The signal-to-noise ratio is estimated to be 1:110 in the case of Fig. 5(a): this may be considered as a lower limit for the polarization ratio. A smaller value is found for Fig. 5(b), for which the S/N ratio is only 50 (because background fluctuations are higher ± 0.03). Incidentally, the theoretical prediction is of the order of 1:170. By comparison, the signal-to-noise ratio obtained with the circular aperture tip is of the order of 10 (Fig. 5(c)).

The resolution ability of the BNA has been estimated by comparing the experimental images obtained with the nanoantenna to the simulation of the electric intensity of the SBM convoluted with the vectorial impulse response (VIR) of the BNA-on-tip. The VIR of the BNA-on-tip is obtained by computing (FDTD-3D) the image accumulated by the probe during the scan of a single electric dipole oriented along the metal triangles of the nanostructure [38]. The VIR for which the theoretical plots fit the experimental ones gives a direct indication onto the resolution of the real BNA used in the experiments. The dotted curves of Fig. 5(a) and Fig. 5(b) represent the convolution of (a) $|E_x|^2$ along *x*-axis, and (b) $|E_y|^2$ along *y*-axis, with the VIR simulated for a BNA of gap size equal to 50 nm. The good agreement between theoretical and experimental results shows that the gap size of the BNA used in the experiments is about 50 nm and its resolution ability is better than $\lambda/20$. Note that resolution estimation is possible since the nanoprobe does not perturb the near-field. In the presence of phase singularities in the probed fields, resolution estimation can become problematic [41, 42]. In our case where a phase singularity is present at the center of each unit cell of the photonic crystal, we took care to not consider the optical phase as a critical parameter for estimating the resolution. We only considered phase-independent intensity distributions.

Another important point is that the resonant properties of the BNA enhance dramatically the collection efficiency of the SNOM probe. The level of collected signal was estimated to be two orders of magnitude higher with the BNA than with a 200 nm wide circular aperture. The fact that these nano-apertures have been opened at the end of the same kind of tips demonstrates that the different collection efficiencies are due to the apertures and not to strong discrepancies of the tip shapes. Note that the area of the BNA (about 0.0268 μm^2) is in our case smaller than the area of the circular aperture (about 0.0314 μm^2). This demonstrates that the outstanding collection efficiency of the BNA can be only due to its resonant antenna effect. Unlike circular nano-aperture usually employed as nanoprobe in near-field optical microscopy, BNAs can reach nanometer resolution with excellent signal-to-noise ratios. Therefore, BNAs may overpass circular apertures in the optimization of optical transmission for SNOM [43]. Such a behavior is in agreement with the theory of BNA (and more generally, of gap-based nanoantennas) which state that decreasing gap size results in a higher capacitive effect which yield a larger dipole moment. Therefore, any increase of resolution ability of the BNA probe (due to a decrease of the gap size) is accompanied by an increase of collection efficiency. In this context, BNA tips allow for overcoming one of the main limitations of SNOM linked to the well-known trade-offs between resolution and signal-to-noise ratio. The strength of the dipole moments of circular apertures small compared to the wavelength is a decreasing function of the aperture size [14].

#158651 - $15.00 USD Received 23 Nov 2011; revised 26 Jan 2012; accepted 31 Jan 2012; published 3 Feb 2012

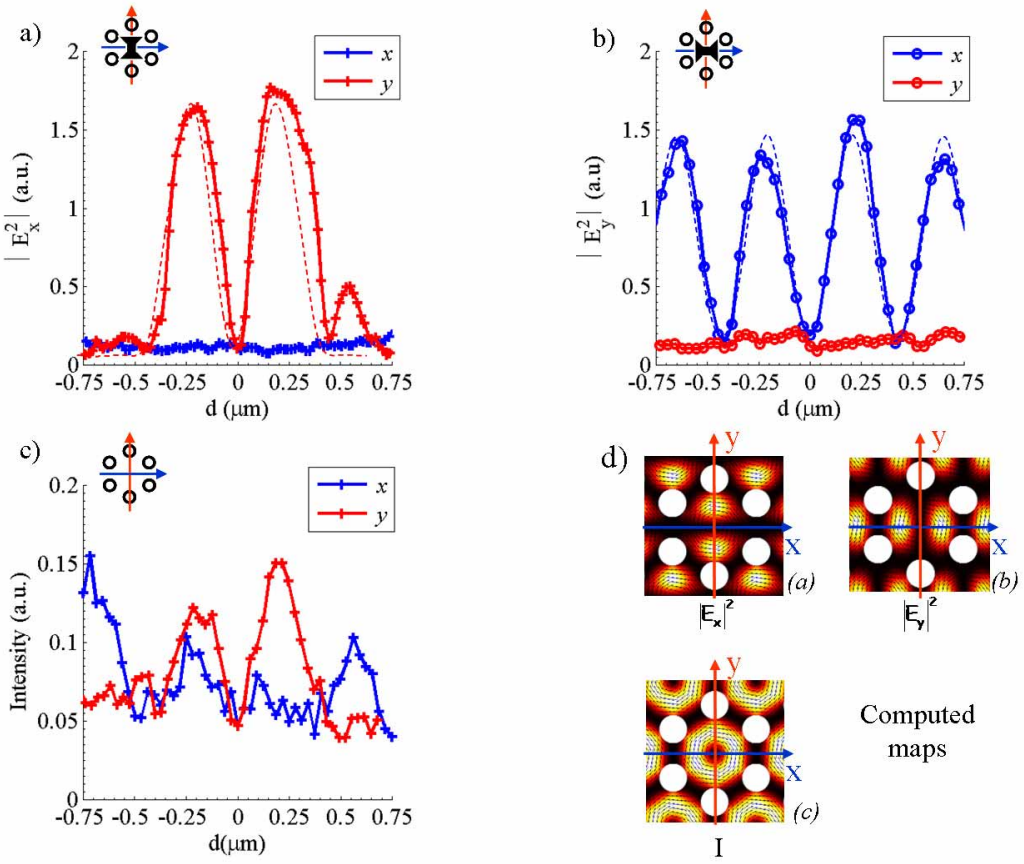

Fig. 5. (a,b) Cross-sections along *x*-axis (in blue) and *y*-axis (in red solid) of the near-field signal collected across a unit cell by a BNA tip oriented (a) along the *x*-axis (cross) and (b) along the *y*-axis (circle) (see figure insets). Dotted curves in (a) and (b): convolution between the simulation of the electric intensity ((a): $|E_x|^2$ along the *x*-axis, (b): $|E_y|^2$ along the *y*-axis) and the vectorial impulse response of the BNA tip. (c) Cross-sections of the intensity along *x*-axis (in blue) and *y*-axis (in red) of the near-field image detected across the same unit cell as in (a,b) with a 200 nm diameter circular aperture tip. (d) Computed maps in one unit cell corresponding to $|E_x|^2$ (a),$|E_y|^2$(b) and $|E_x|^2+|E_y|^2$ (c).

#158651 - $15.00 USD Received 23 Nov 2011; revised 26 Jan 2012; accepted 31 Jan 2012; published 3 Feb 2012

5. Conclusion

In conclusion, we have used a bow-tie aperture nanoantenna (BNA) to perform a local, near-field optical probing of the electric field polarization of a slow Bloch laser mode (SBM) in a photonic crystal. The high sensitivity of the BNA to the electric field and its polarization filtering properties yield optical near-field probes with a high spatial resolution and an enhanced collection efficiency compared to conventional, metal coated optical fiber probers. The BNA probe's ability to discriminate between near-field polarization states on a subwavelength scale has been demonstrated by measuring the experimental SBM spatial profile and comparing it to 3D FDTD simulations. An excellent agreement was found which highlights the fact that the BNA near-field probe does not generate any significant perturbation of the optical mode of the photonic crystal. We have also shown that the BNA can overcome one of the main limitations of SNOM, linked to the well-known trade off between resolution and signal-to-noise ratio. In future studies, the coupling of BNA probes with heterodyne detection SNOM would allow for the full vectorial characterization of optical modes at the surface of PCs, for both the electric and magnetic fields [38]. The present investigation also paves the way for emerging nanophotonic architectures aiming at integrating nanoantennas [44, 45] on top of a PC resonator. Nanoantenna-on-fiber devices could also be seen as an optimized interface for out-coupling optical energy from PC structures toward fiber networks.

Acknowledgments

This work is funded by the "Agence Nationale de la Recherche" under contract n°ANR07-NANO-036. It is supported by the "Pôle de compétitivité Microtechnique". Support from the NSW Intersect merit allocation program is acknowledged. The authors are indebted to J.-Y. Rauch and D. Troadec for support in the fabrication of the BNAs and Ph. Regreny for growing the epitaxial structures. The nanoantennas integrated on fiber tips were fabricated at MIMENTO and IEMN technology platforms. The wafer bonding technology was performed by E. Augendre and L. Di Cioccio at CEA-LETI. The authors acknowledge the technological support at NANOLYON facility.

#158651 - $15.00 USD Received 23 Nov 2011; revised 26 Jan 2012; accepted 31 Jan 2012; published 3 Feb 2012